TECHNICAL PAPER

Fluid structure interaction (FSI) simulation of the left ventricle (LV) during the early filling wave (E-wave), diastasis and atrial contraction wave (A-wave)

Md. S. Arefin · Yosry S. Morsi

Abstract In this paper, the hemodynamic characteristics inside a physiologically correct three-dimensional LV model using fluid structure interaction scheme are examined under various heart beat conditions during early filling wave (E-wave), diastasis and atrial contraction wave (A-wave). The time dependent and incompressible viscous fluid, nonlinear viscous fluid and the stress tensor equations are coupled with the full Navier–Stoke's equations together with the Arbitrary Lagrangian–Eulerian and elasticity in the solid domain are used in the analysis. The results are discussed in terms of the variation in the intraventricular pressure, wall shear stress (WSS) and the fluid flow patterns inside the LV model. Moreover, changes in the magnitude of displacements on the LV are also observed during diastole period. The results obtained demonstrate that the magnitude of the intraventricle pressure is found higher in the basal region of the LV during the beginning of the E-wave and A-wave, whereas the Ip is found much higher in the apical region when the flow propagation is in peak E-wave, peak A-wave and diastasis. The magnitude of the pressure is found to be 5.4E2 Pa during the peak E-wave. Additionally, WSS elevates with the rise in the E-wave and A-wave but the magnitude decreases during the diastasis phase. During the peak E-wave, maximum WSS is found to be 5.7 Pa. Subsequent developments, merging and shifting of the vortices are observed throughout the filling wave. Formations of clockwise vortices are evident during the peak E-wave and at the onset of the A-wave, but counter clockwise vortices are found at the end of the diastasis and at the beginning of the A-wave. Moreover, the maximum magnitude of the structural displacement is seen in the ventricle apex with the value of 3.7E−5 m.

Introduction

The fluid structure interaction (FSI) method is extensively used to investigate and analyse the complete operational activities of the heart. This scheme is applied to determine the entire functionalities and physiological changes in the whole cardiac structure which includes the heart valves [1–5], arteries [6–10] and ventricles [11–15]. Additionally, this method is also utilized for the cardiac investigation and electrical initiation, mechanics, metabolism and fluid mechanics of the ventricles [16–22].

The hemodynamics inside the left ventricle of the heart has been extensively investigated by many researchers over the last few decades. In 1981, Reul et al. [23] investigated the development of vortices initiating by strong pressure gradient for the LV contraction. Later, Taylor et al. [24] investigated the three dimensional LV ejection using computational fluid dynamics (CFD). However, generation of vortices and the displacement of the ventricle wall were not examined properly. After that, Vierendeels et al. [25] developed a two dimensional canine LV model and analysed the flow patterns and the changes in the intraventricular pressure inside the cavity during diastole stage but they did not consider the effect of ventricle wall.

In the following year, McQueen and Peskin [21] introduced a novel numerical method, namely Immersed

Md. S. Arefin (✉) · Y. S. Morsi
Biomechanical and Tissue Engineering Laboratory, Swinburne University of Technology, Hawthorn, VIC 3122, Australia
e-mail: marefin@swin.edu.au

Y. S. Morsi
e-mail: ymorsi@swin.edu.au

Boundary Method which is a coupling mechanism used to couple the interaction between the fluid and solid domain. By using this technique they investigated the flow dynamics inside the whole heart, incorporating the left and right ventricle. Afterwards, using the data from [21], Lemmon and Yoganathan [26] used FSI to further investigate the diastolic functionalities of the LV including the atrium and pulmonary veins under various conditions of ventricle dysfunction. Other studies investigated the hemodynamics of the LV including the generation of vortices and the changes in the intraventricular pressure by using simplified LV structure [27, 28], magnetic resonance imaging [29, 30] and electromechanical models [31–35].

Subsequently, Watanabe et al. [36] simulated the flow pattern inside the LV during the filling phase without considering the total anatomical features and neglecting the dynamic characteristics of the ventricle rigidity. Later, Cheng et al. [13] simulated the flow pattern and the intraventricular pressure changes inside the LV under the filling phase but again the original ventricle-wall properties were discarded. Similarly the three-dimensional (3D) filling flow inside the left ventricle has been simulated by Domenichini et al. [37] whereas, Pedrizzetti and Domenichini [38] examined the asymmetric flow distributions numerically within the left ventricle assuming that the mitral valve is circular and wide-open. Afterwards, a review of the previous researches with particular emphasis on the coupling mechanisms including the contraction, activation and ventricular blood flow inside the heart was reported by Lee et al. [39], concluding that to date the total physiological details have not yet fully incorporated in previous research. Consequently, Nordsletten et al. [40] reviewed the mathematical structure of LV for demonstrating the mechanical expansion and contraction of the ventricles along with the functioning properties of the heart. Lassila et al. [41] considered patient-specific case in developing a model of LV and carried out a numerical analysis using FSI method. However, they did not consider the ideal boundary conditions in the 3D interface of the LV model.

All the previous investigations mostly focused on the general flow pattern inside the model of LV with varying degree of success. However, a complete analysis of the hemodynamics and structure of the LV to determine the variations in the hemodynamic forces and intraventricular pressure distribution is not thoroughly discussed. Therefore, in this paper we use FSI to determine the hemodynamic characteristics inside the LV during the filling phase under various physiological conditions. Variations in the intraventricular pressure change, wall shear stress (WSS) and flow pattern including the generation, evolution and merging of vortices are fully analysed. Moreover, the deformation of the structure is presented in terms of total mesh displacement (TMD) of the LV model during the diastole condition.

Mathematical procedure

Primary conditions for the fluid-flow related problems are usually computed by using the principles of conservation of mass, momentum and energy equations. The governing equations are mathematically discreted by means of finite element based methods and subsequently the Navier–Stokes equations for the time-dependent incompressible viscous fluid coupled with the continuity equation, are used in the simulation [42]:

$$\frac{\partial p}{\partial y} + \frac{\partial(\rho Vx)}{\partial x} + \frac{\partial(\rho Vy)}{\partial y} + \frac{\partial(\rho Vz)}{\partial z} = 0 \qquad (1)$$

The momentum equations are given as [42]:

$$\frac{\partial \rho v_x}{\partial t} + \frac{\partial(\rho v_x v_x)}{\partial x} + \frac{\partial(\rho v_y v_x)}{\partial y} + \frac{\partial(\rho v_z v_x)}{\partial z} = \rho g_x - \frac{\partial P}{\partial x} + R_x \\ + \frac{\partial}{\partial x}\left(\mu_e \frac{\partial v_x}{\partial x}\right) + \frac{\partial}{\partial y}\left(\mu_e \frac{\partial v_x}{\partial y}\right) + \frac{\partial}{\partial z}\left(\mu_e \frac{\partial v_x}{\partial z}\right) \qquad (2)$$

$$\frac{\partial \rho v_y}{\partial t} + \frac{\partial(\rho v_x v_y)}{\partial x} + \frac{\partial(\rho v_y v_y)}{\partial y} + \frac{\partial(\rho v_z v_y)}{\partial z} = \rho g_y - \frac{\partial P}{\partial y} + R_y \\ + \frac{\partial}{\partial x}\left(\mu_e \frac{\partial v_y}{\partial x}\right) + \frac{\partial}{\partial y}\left(\mu_e \frac{\partial v_y}{\partial y}\right) + \frac{\partial}{\partial z}\left(\mu_e \frac{\partial v_y}{\partial z}\right) \qquad (3)$$

$$\frac{\partial \rho v_z}{\partial t} + \frac{\partial(\rho v_x v_z)}{\partial x} + \frac{\partial(\rho v_y v_z)}{\partial y} + \frac{\partial(\rho v_z v_z)}{\partial z} = \rho g_z - \frac{\partial P}{\partial z} + R_z \\ + \frac{\partial}{\partial x}\left(\mu_e \frac{\partial v_z}{\partial x}\right) + \frac{\partial}{\partial y}\left(\mu_e \frac{\partial v_z}{\partial y}\right) + \frac{\partial}{\partial z}\left(\mu_e \frac{\partial v_z}{\partial z}\right) \qquad (4)$$

where, V_x, V_y and V_z are considered as the components of the velocity vectors in the cartesian co-ordinates of X, Y and Z respectively; ρ and μ represent the density and dynamic viscosity respectively.

For the elastic in the solid domain, the motion equation for displacement is used and presented as [43]:

$$\nabla \cdot \sigma + f = 0 \qquad (5)$$

where, σ denotes the stress tensor and f is the body force.

Moreover, assuming small deformation the following equation for the stress tensor is adapted [43]:

$$\sigma = \frac{E}{1+\upsilon}\left(\frac{\upsilon}{1-2\upsilon}\mathrm{tr}(\varepsilon)\mathrm{I} + \varepsilon\right) - \frac{E}{1-2\upsilon}\alpha(T-T_0)\mathrm{I} \qquad (6)$$

where, E is the young's modulus, υ is the Poisson's ratio, T is the temperature, T_0 is the reference temperature and I is unit tensor.

In this study the Arbitrary Lagrangian–Eulerian (ALE) finite-element method is expressed to compute the non-linear viscous fluid on large free surface wave function. It is to be noted that when the ALE method is compared to its
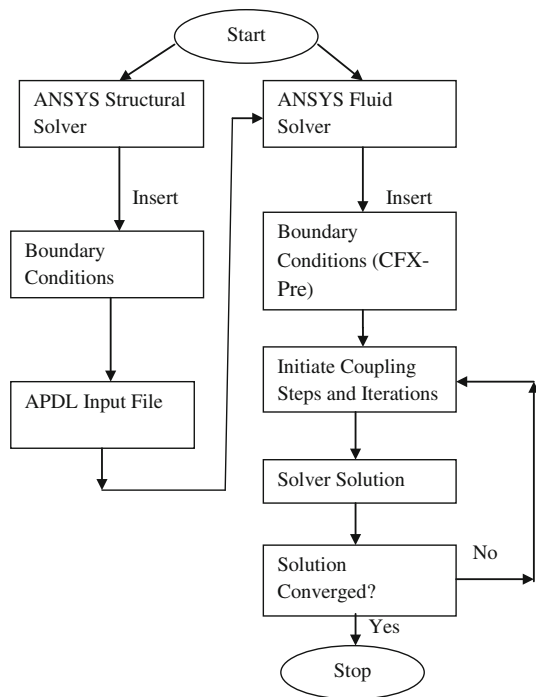
Fig. 1 Flow chart for the LV simulation procedure

Fig. 2 Sketch of the left ventricle (LV) model constructed using SolidWorks, (2010)

Eulerian counterparts, it offers comprehensive solution accuracy for those structures which can deform and comprise fluid. Full account of the use of ALE based on the Navier–Stoke's equation is given in [42, 44, 45]. The flow chart shown in Fig. 1 illustrates the conditions for the simulation convergence during the entire simulation. Semi-Implicit Method for Pressure Linked Equations (SIMPLE) algorithm is implemented here to compute the mass and momentum equations [26, 46]. Figure 1 also shows the unidirectional FSI algorithm as a flow chart for the entire computational procedure till the convergence of the simulation occurred.

In the present study, ANSYS 15.0 has been used to compute the entire simulation by carrying out the following steps: initially, the material density and the isotropic characteristics are inserted into the geometry; subsequently, the meshing is computed by using the ALE equations and then the coupling procedure is selected. It should be noted that throughout the filling phase, 0.5 s is used as the total time duration as recommended in [13].

Computational procedure

Geometry

Even though a simplified model is utilized for this diastolic-simulation, but it has been reported in literature, if one
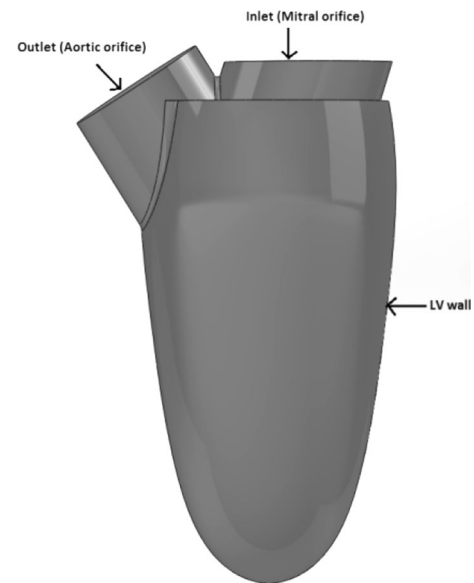
carefully allocates the necessary structural and hemodynamic boundary conditions the utilization of a simplified LV model is sufficient to generate accurate results that are comparable to the real cases of LV [12, 13, 28, 36]. Also, the simulated model (Fig. 2) is obtained by taking the complete physiological features of the left ventricle by depending on the convenience of using the magnetic resonance imaging (MRI) data and the medical textbook data. The prescribed dimensions are close to the realistic LV data [12, 35, 47, 48].

The shape of the geometry, shown in Fig. 2 is an ellipsoidal, with the magnitude of 0.7 cm starting from the top (inlet) to the bottom (apex) and the value of 3.6 cm from right to left of the LV. In line with the work of Cheng et al. [13], the inlet/mitral orifice, which contains the mitral valve of 2.5 cm in diameter, is considered wide open. Alternatively, the outlet/aortic orifice which comprises the aortic valve, with the diameter of 2.1 cm is assumed to be fully closed during the entire simulation. Moreover, the heart wall is assumed to contain a uniform wall thickness with the value of 0.1 cm.

Boundary conditions

The inlet velocity flow profile has been accumulated from a lumped parameter model, where the data is clinically collected from an adult, who is young and healthy. The obtained data was further modified from the model of Waite et al. [49] as shown in Fig. 3. Figure 3 demonstrates the transmitral flow velocity (U) (in m/s) against the time
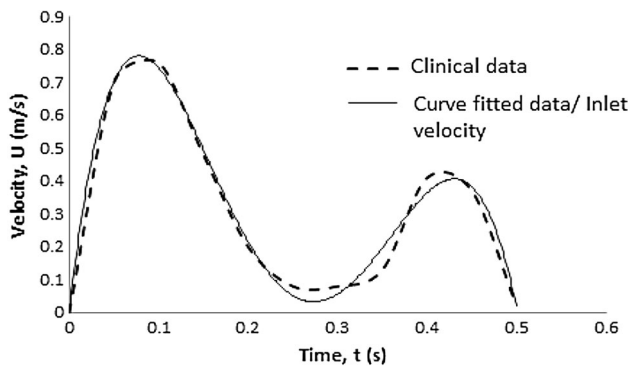
Fig. 3 Inlet: transmitral flow velocity (U) versus the time (t) curve

Fig. 4 Mesh independency test

(t) (in seconds) curve, which is given as the inlet boundary condition. Curve-fitting procedure has been undertaken to obtain the velocity curve for the inlet, where the curve matches 96 % with the original one obtained from [13, 49].

Moreover, the native wall of heart is assumed to be isotropic and homogenous with the density of the ventricle wall prescribed to be 1.2 g/cm^3, elastic modulus of 0.7 MPa and the Poisson's ratio of 0.4. The fluid flow is considered to be Newtonian with the density of 1,050 kg/m^3 and the viscosity of 0.0035 Pa s including the no-slip boundary conditions and the flow is assumed to be laminar [13, 25, 41]. This simulation has been performed by Intel® Xeon® processor of 3.07 GHz.

Meshing statistics and mesh independency test

Initially, the CAD model of the LV is imported into AN-SYS 15.0, where the meshing is performed and the required boundary conditions are implemented. Mapped face meshing is executed individually for both the solid and the fluid domains. Moreover, the line control properties are implemented in order to obtain the variation in the fluid velocity. Consequently, a mesh independency test is performed using these line control properties by comparing the variations in fluid velocity for subsequent nodes and elements [1]. These variations are computed until the fluid velocity is converged. Figure 4 illustrates the mesh independency test on fluid velocity. Three different types of mesh (coarse, medium and fine) statistics have been utilised and varied throughout the simulation. It is verified that the 19,706 nodes and 10,058 elements for the structural and 138,311 nodes and 746,829 elements for the fluid region are considered to be ideal for this analysis. Subsequently, for this simulation, these nodes and elements are adopted for the medium mesh type. It is to be noted that the convergence criterion for the fluid flow is set to be 10^{-4} and for the coupling data transfer it is taken as 10^{-2}.
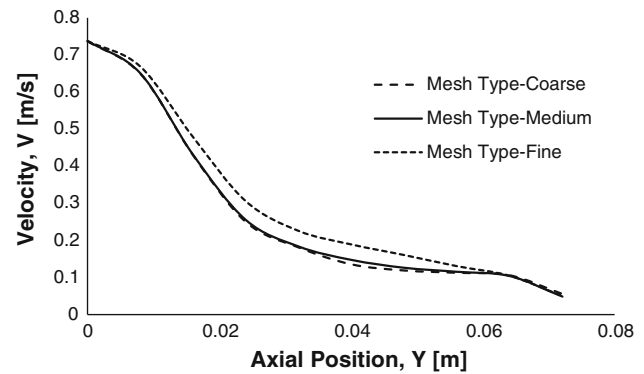
Results and discussion

The results are presented here in terms of intraventricular pressure distribution, wall shear and flow dynamics comprising the generation, evolution and merging of vortices inside the LV during the early filling wave (E-wave), diastasis and atrial contraction wave (A-wave). Moreover, changes in the deformation of the LV structure are presented in terms of TMD during the diastolic flow.

Pressure distributions

It is to be recognised that as shown in Fig. 3, there are two peaks that can be found; for example, when $t = 0.08$ s the transmitral velocity (U) is nearly 0.8 m/s, and the other one, when $t = 0.44$ s the velocity (U) is approximately 0.4 m/s. The first peak is known as the early filling wave (E wave), which occurs during the resting-period of the ventricle as the blood enters inside the left ventricle from the left atrium and the second peak is denoted as the atrial contraction wave (A wave), which is responsible for exerting the pressure on the atria. Moreover, within these two peaks, the mid phase of the filling wave (approximately $0.22 < t < 0.3$ s) is known as the diastasis or slow/relaxed filling phase [13].

Figure 5 demonstrates the pressure distribution inside the LV where the variations in the intraventricular pressure is distinguished by taking a XY cross sectional plane during the filling cycle. The changes in the pressure distribution are shown for seven different time steps and are determined as stated above by considering the mitral valve (inlet) wide-open and the aortic valve (outlet) completely closed [13].

From Fig. 5, at the beginning of the filling wave the fluid starts to enter through the inlet into the LV and when, $t = 0.025$ s the inlet velocity is 0.3 m/s and the magnitude in the basal pressure (near the inlet) is found to be much

(a) t= 0.025s   (b) t= 0.075s   (c) t= 0.15s

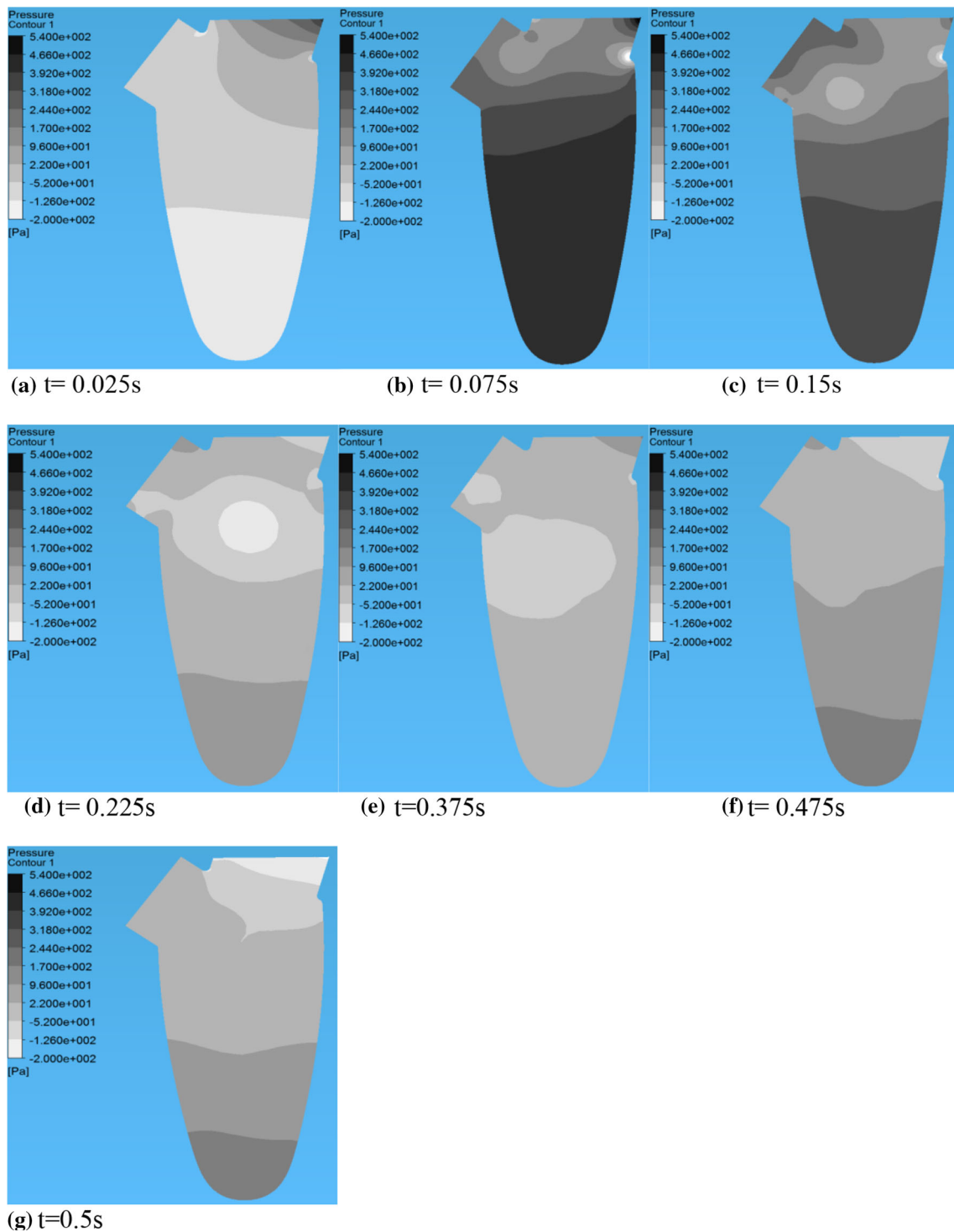(d) t= 0.225s   (e) t=0.375s   (f) t= 0.475s

(g) t=0.5s

Fig. 5 Variation of pressure of the LV in different time steps.

higher than the apical pressure. During this time step, a negative pressure gradient is formulated in the apical region of the ventricle, as the inlet velocity has not reached to its apex yet. When the inlet wave (approximately 0.8 m/s) reaches its peak ($t = 0.075$ s, peak E-wave) the

intraventricular pressure increases inside the ventricle chamber and the magnitude of the pressure is found to be around 5.4E2 Pa in the ventricle apex. Moreover, it is observed that the apical region of the ventricle contained more pressure compared to the basal region of the ventricle

during the peak E-wave. Furthermore, a vortex is observed near the outflow tract.

After reaching the peak of the E-wave, inlet velocity starts to decrease to approximately 0.5 m/s at $t = 0.15$ s and the variation in the intraventricular pressure is found to be higher in the ventricle apex than the basal region.

During the same time step, the previous vortex which is found near the outflow tract, starts to enlarge and shifts its position towards the centre of the LV. Moreover, when the intraventricular pressure reached at the apical region of the ventricle, tip of the LV wall provided a positive reflection back to the inflow wave. The mixing of these
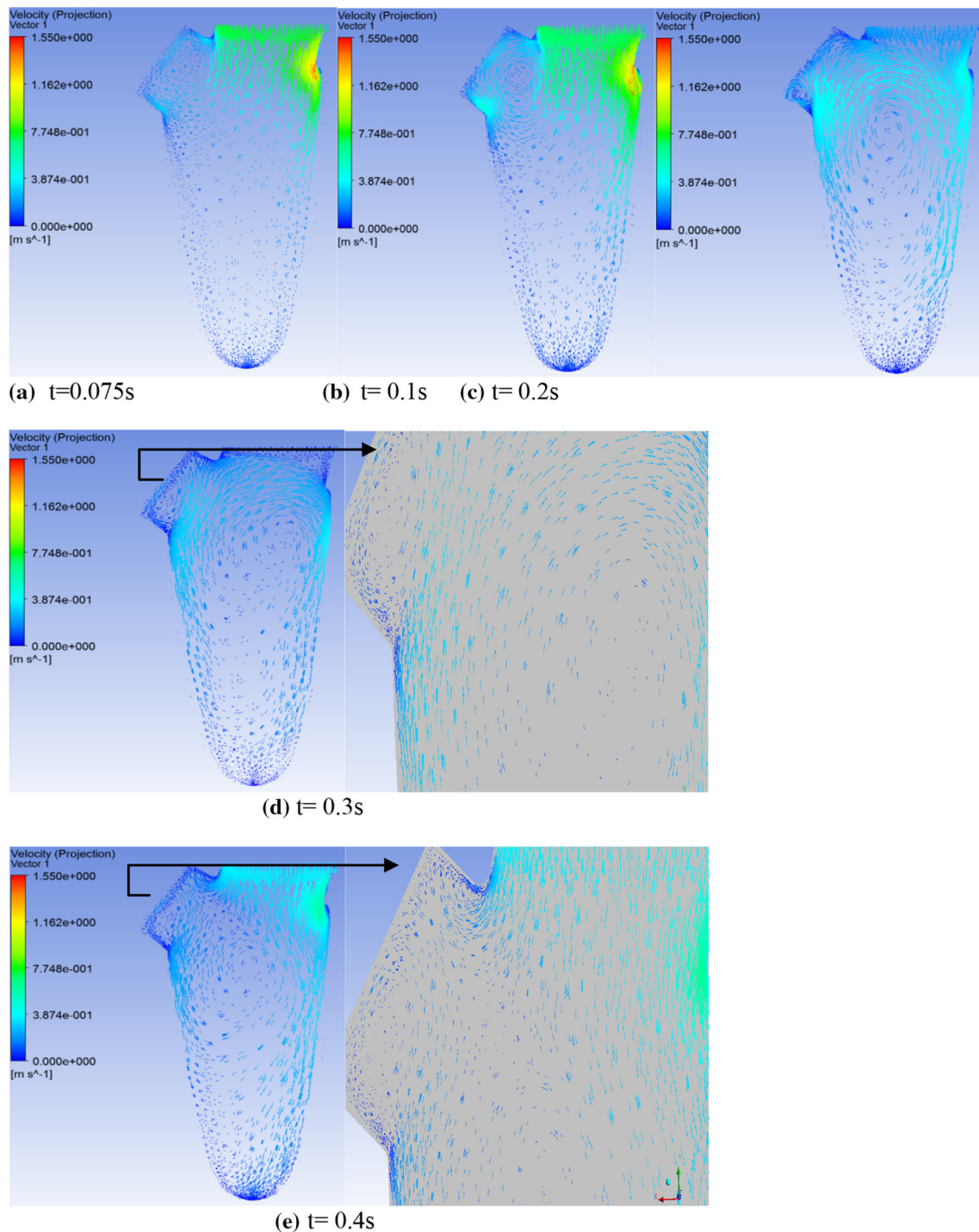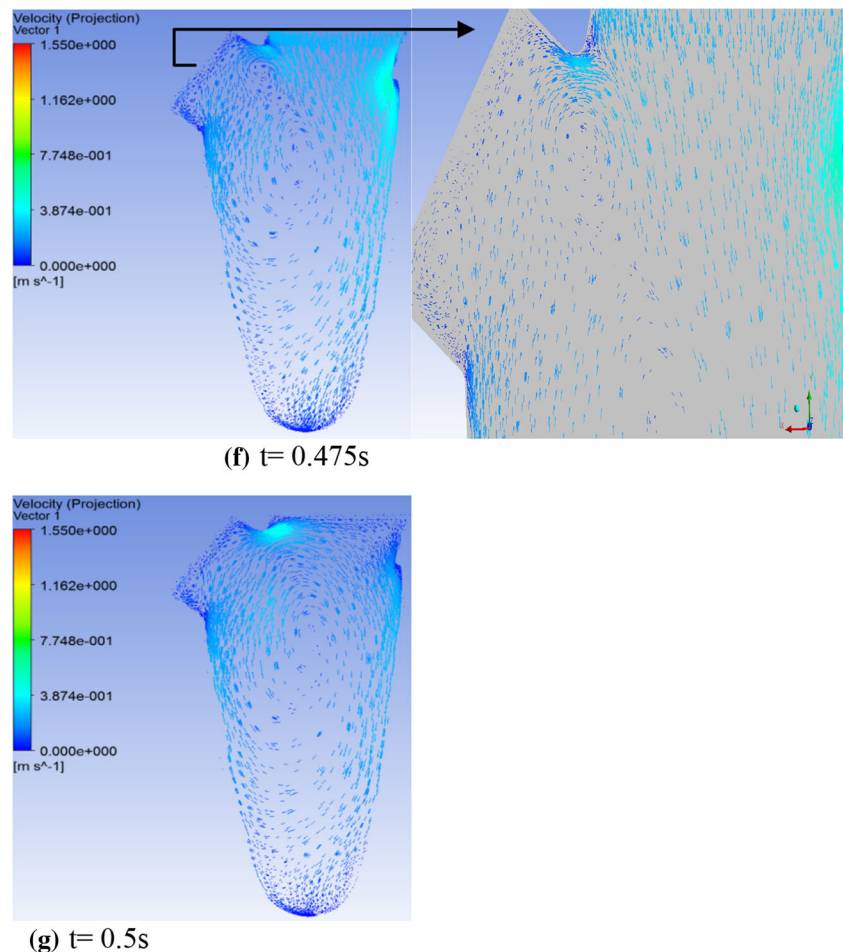

(a) t=0.075s   (b) t= 0.1s   (c) t= 0.2s

(d) t= 0.3s

(e) t= 0.4s

Fig. 6 Velocity distribution of the LV in different time steps.

Fig. 6 continued

(f) t= 0.475s

(g) t= 0.5s

two waves elevated the apical pressure and generated the F-wave [13].

Still during the diastasis, inlet velocity decelerates and the changes in the intraventricular pressure are also evident inside the LV. With the velocity of 0.1 m/s (when $t = 0.225$ s) magnitude of the apical pressure is found to be much higher than the basal pressure. Moreover, the vortex is seen developed in the centre of the LV chamber and a new vortex starts to form near the outlet region. Once more, with the rise in the inflow velocity (when $t = 0.375$ s) basal pressure starts to elevate again more than that of the apical region of the ventricle. A second vortex is seen forming near the outlet, while the primary vortex slowly starts to merge with the inflow wave. As a result, with the rise in the inflow velocity the vortex slowly starts to merge inside the chamber.

Subsequently, at the onset of the A-wave basal pressure rises once again more than the apical pressure but when it reaches the peak of the A-wave, magnitude of the pressure in the apex is found to be higher again than the basal pressure. At the end of the filling wave ($t = 0.5$ s) magnitude of the basal pressure elevates slightly but it is still lower than the apical pressure.

The general trends of the intraventricular pressure distribution, starting from the base to apex and formulation of vortices during the filling wave inside the LV are found to be in line with the findings of the previous studies [13, 25, 28].

It is to be noted that LV filling pressure can be computed intrusively mainly in three different ways as, (i) mean pulmonary wedge pressure (MPWP) or mean left atrial (LA) pressure, (ii) left ventricular end-diastolic pressure (LEDP), which is after the initiation of the A-wave pressure and (iii) pre-A left ventricular diastolic pressure. In order to examine the LV-diastole in detail, the transmitral pressure flow relation plays a vital role and this relationship can be found in detail in open literature [50, 51].

Furthermore, WSS has also been computed to examine its influence on the wall motion. It is found that with the rise in the inflow velocity WSS elevates and the magnitude decreases when it is in the diastasis phase. At the onset of the A-wave WSS rises once again due to the higher inflow wave than the diastasis. Still during the peak of the E-wave, diastasis and A-wave the magnitude is found around 4, 1.38 and 1.63 Pa respectively in the apical region and in the basal region, it is of 5.7, 1.4 and 2 Pa respectively.
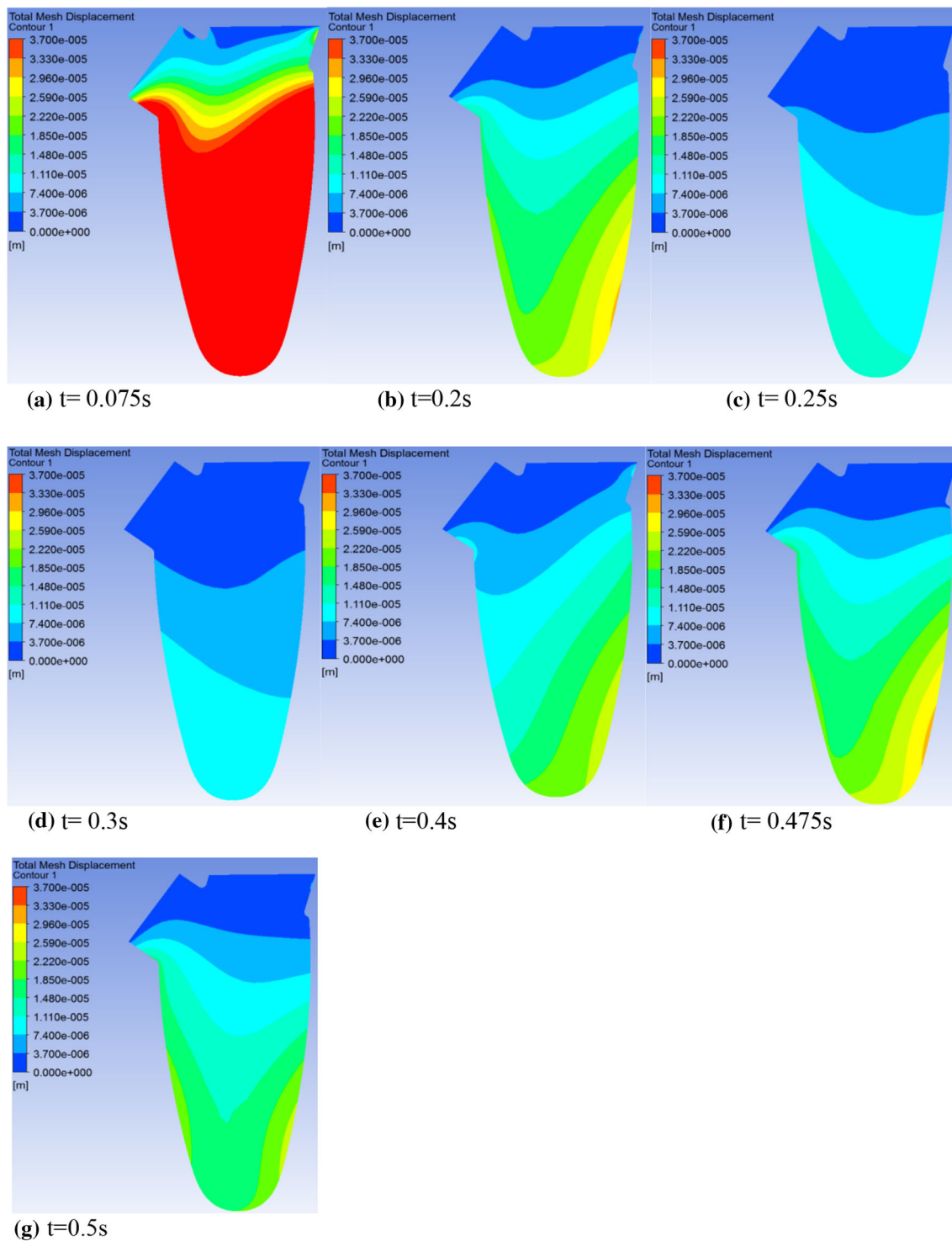
Fig. 7 Total mesh displacement of the LV using contour during the filling period.

Velocity distributions

The characteristics of the flow pattern inside the left ventricle are also illustrated in Fig. 6. The XY cross sectional plane in

the LV using velocity vectors during the filling phase is taken. Similar to the pressure distribution, velocity mapping is also shown by taking the wide-open inlet and completely closed outlet for the same time steps investigated here.

At the beginning of the filling wave (Fig. 3), the fluid starts to enter into the LV and when it reaches the peak of the E-wave ($t = 0.075$ s) maximum inflow jet (around 0.8 m/s) is progressed through the inlet and the fluid continues to flow from the base to the apex. The E-wave causes a ring shaped, clockwise (CW) vortex near the dead-end of the outlet region to be formed. Moreover, it is observed that higher velocity is found in the anterior region of the LV than the posterior side from the inlet. After reaching the peak of the E-wave, inflow velocity starts to decrease and due to this the adherence vortex which is formed earlier shifts its position a little from the outlet and starts to enlarge at the same time. Subsequently, the magnitude of the inflow velocity (0.2 m/s) further decreases when the time step is in $t = 0.2$ s and from Fig. 6c, the shape of the vortex elongates and moves to the centre of the ventricle chamber. At the end of the diastasis phase, the vortex starts to enlarge once again but another counter-clockwise (CCW) vortex is seen formulated at the anterior region of the outlet.

At the onset of the A-wave, the vortex shifts its position once again (Fig. 6e) due to the rise in the inlet velocity and the CCW vortex also starts to enlarge simultaneously. A third vortex which is CW, is seen to be developed in the vicinity of the inlet and the outlet region. At the peak of the A-wave, inlet velocity starts to elevate again and due to this, the primary vortex starts to merge inside the LV. After reaching the peak of the A-wave, inlet velocity decreases again and during the time step $t = 0.475$ s the second vortex remains near the outlet region but the weak third vortex shifts its location a little towards the centre of the LV. At the end of the filling phase ($t = 0.5$ s) the weak third vortex completely merges with the propagation of the inflow fluid and a primary vortex is established again at the centre of the ventricle chamber. There the maximum velocity of 1.55 m/s is obtained during the diastolic phase.

The general trends regarding the flow pattern, development, shifting and mixing/merging of vortices are again in line with the findings from previous studies [13, 25, 27, 28, 36, 41]. Furthermore, the formation of the vortices observed here also matches with the work from Cheng et al. [13], but the progressions of those vortices reported by Cheng's group do not directly match with the current observations. This can be attributed to the fact that during the late diastole-phase the flow pattern predicted can be different due to the use of various computational/simulation procedure.

Structure simulation and total mesh displacement

Similarly, TMD is also observed by taking a XY cross-sectional plane inside the LV. Figure 7 demonstrates the TMD by considering the completely opened inlet and completely closed outlet for the same time step as the pressure and velocity distributions discussed above.

At the onset of the filling phase, the volume starts to increase inside the LV and after certain time-period, for example, at the peak of the E-wave, fluid enters into the LV with maximum velocity through the inlet and because of this, much higher displacement is found in the apical region than the basal region of the LV. Moreover, as the inlet velocity enters into the diastasis phase, the magnitude of the TMD minimises in the tip of the LV and when $t = 0.25$ s, the displacement shifted from the posterior side to its anterior side in the apical region of the ventricle-contour.

The inlet velocity starts to rise again during the initiation of the A-wave and because of this magnitude of the TMD is found to be higher again in the apical region. After reaching the peak of the A-wave, propagation of the inflow velocity decelerates and due to this, the magnitude of the displacement is found to be higher once more in the apical region. It indicates that the change in the intraventricular pressure inside the LV wall and at the end of the filling wave ($t = 0.5$ s), the displacement shifts a little further as the inlet velocity reduces.

This TMD is only taken into the XY-contour plot. However, for different contour plots in different positions will result different TMD. These simulations provide better ideas and conditions for the LV during the filling phase.

Conclusion

In this study, the simulations show that the changes in Ip inside the ventricle occurred because of the variation in the ventricle wall during early filling wave and atrial contraction wave. Consequently, the magnitude of the intraventricular pressure is found to be much higher than the basal pressure during the peak of the E-wave, A-wave and diastasis but basal pressure is found to be higher during the initiation of the E-wave and A-wave. Subsequently, WSS elevates with the rise in the flow propagation of the E-wave and the A-wave, but vice versa during the diastasis. Moreover, generation and shifting of vortices are evident inside the ventricle during the transmitral velocity flow but depending on different simulation approaches the flow pattern can vary during the late-diastole stage. These cardiac conditions primarily match and agree well with the results from previous studies and clinically observed results, which substantially highlight the true insights of the flow dynamics, intraventricular pressure changes and the structural displacement during the diastolic phase. Furthermore, the maximum magnitude of the Ip is found to be 5.4E2 Pa, WSS of 5.7 Pa with the velocity of 1.55 m/s. Subsequently, maximum displacement of 3.7E−5 m is

found mainly in the apical region of the LV during the peak of the E-wave. Although there are some limitations in the present work, it still provides sufficient insights particularly related to the variations in the intraventricular pressure, WSS, flow velocity and TMD. Further experimental investigations are currently planned at our laboratory, using particle image velocimetry (PIV) and laser Doppler anemometers (LDA) to obtain a good quantitative data for verification and validation of the numerical predictions.

References

1. Kouhi E (2011) An advanced fluid structure interaction study of tri-leaflet aortic heart valve. Swinburne University of Technology, Melbourne

2. De Hart J, Peters GWM, Schreurs PJG, Baaijens FPT (2000) A two-dimensional fluid–structure interaction model of the aortic value. J Biomech 33(9):1079–1088. doi:10.1016/S0021-9290(00)00068-3

3. Morsi YS, Yang WW, Wong CS, Das S (2007) Transient fluid–structure coupling for simulation of a trileaflet heart valve using weak coupling. J Artif Organs 10(2):96–103. doi:10.1007/s10047-006-0365-9

4. Marom G, Peleg M, Halevi R, Rosenfeld M, Raanani E, Hamdan A, Haj-Ali R (2013) Fluid–structure interaction model of aortic valve with porcine-specific collagen fiber alignment in the cusps. J Biomech Eng 135(10):101001–101006. doi:10.1115/1.4024824

5. Kemp I, Dellimore K, Rodriguez R, Scheffer C, Blaine D, Weich H, Doubell A (2013) Experimental validation of the fluid-structure interaction simulation of a bioprosthetic aortic heart valve. Australas Phys Eng Sci Med 36(3):363–373. doi:10.1007/s13246-013-0213-1

6. Kouhi E, Morsi Y, Hassan Masood S (2008) Two way FSI analysis of CABG with physiologically realistic pulsatile flow and nonlinear artery structure. J Biomech 41:S245

7. Morsi Y, Owida A, Do H, Arefin MS, Wang X (2012) Graft-artery junctions: design optimization and CAD development. In: Liebschner MAK (ed) Computer-aided tissue engineering. Methods in molecular biology, vol 868. Humana Press, Totowa, pp 269–287. doi:10.1007/978-1-61779-764-4_16

8. Do HV (2012) Design and optimization of coronary arteries bypass graft using numerical method. Swinburne University of Technology, New York

9. Freshwater IJMY, Lai T (2006) The effect of angle on wall shear stresses in a LIMA to LAD anastomosis: numerical modelling of pulsatile flow. Proc Inst Mech Eng H 220(7):743–757

10. Kouhi E, Morsi Y, Masood SH (2009) The effect of arterial wall deformability on hemodynamics of CABG. pp 485–494

11. Ong CW, Chan BT, Lim E, Abu Osman NA, Abed AA, Dokos S, Lovell NH (2012) Fluid structure interaction simulation of left ventricular flow dynamics under left ventricular assist device support. In: 34th Annual international conference of the IEEE EMBS, pp 6293-6296

12. Zheng X, Seo JH, Vedula V, Abraham T, Mittal R (2012) Computational modeling and analysis of intracardiac flows in simple models of the left ventricle. Eur J Mech 35:31–39. doi:10.1016/j.euromechflu.2012.03.002

13. Cheng Y, Oertel H, Schenkel T (2005) Fluid–structure coupled CFD simulation of the left ventricular flow during filling phase. Ann Biomed Eng 33:567–576. doi:10.1007/s10439-005-4388-9

14. Tang D, Yang C, Geva T, Nido PJd (2010) Image-based patient-specific ventricle models with fluid–structure interaction for cardiac function assessment and surgical design optimization. Prog Pediatr Cardiol 30(1–2):51–62

15. Nordsletten D, McCormick M, Kilner PJ, Hunter P, Kay D, Smith NP (2011) Fluid–solid coupling for the investigation of diastolic and systolic human left ventricular function. Int J Numer Methods Biomed Eng 27(7):1017–1039. doi:10.1002/cnm.1405

16. Hunter PJ, Pullan AJ, Smaill BH (2003) Modeling total heart function. Annu Rev Biomed Eng 5:147–177. doi:10.1146/annurev.bioeng.5.040202.121537

17. Khalafvand SS, Ng EYK, Zhong L (2011) CFD simulation of flow through heart: a perspective review. Comput Methods Biomech Biomed Eng 14(1):113–132

18. Lee B-K (2011) Computational fluid dynamics in cardiovascular disease. Korean Circ J 41(8):423–430

19. Versteeg HK, Malalasekera W (2007) An introduction to computational fluid dynamics. The finite volume method, 2nd edn. Pearson, Harlow

20. Tu J, Yeoh GH, Liu C (2008) Computational fluid dynamics: a practical approach. Elsevier, Burlington

21. McQueen DM, Peskin CS (2000) A three-dimensional computer model of the human heart for studying cardiac fluid dynamics. ACM SIGGRAPH Comput Graph 34(1):56–60

22. Ding J, Liu Y, Wang F, Bai F (2012) Impact of competitive flow on hemodynamics in coronary surgery: numerical study of ITA-LAD model. Comput Math Methods Med 2012:7. doi:10.1155/2012/356187

23. Reul H, Talukder N, Müller EW (1981) Fluid mechanics of the natural mitral valve. J Biomech 14(5):361–372. doi:10.1016/0021-9290(81)90046-4

24. Taylor TW, Okino H, Yamaguchi T (1994) Three-dimensional analysis of left ventricular ejection using computational fluid dynamics. J Biomech Eng 116(1):127–130. doi:10.1115/1.2895696

25. Vierendeels JA, Riemslagh K, Dick E, Verdonck P (1999) Computer simulation of left ventricular filling flow: impact study on echocardiograms. Comput Cardiol 1999(1999):177–180. doi:10.1109/CIC.1999.825935

26. Lemmon JD, Yoganathan AP (2000) Computational modeling of left heart diastolic function: examination of ventricular dysfunction. J Biomech Eng 122(4):297–303

27. Verdonck P, Vierendeels J (2002) Fluid–structure interaction modelling of left ventricular filling. In: Sloot PA, Hoekstra A, Tan CJK, Dongarra J (eds) Computational science: ICCS 2002. Lecture notes in computer science, vol 2331. Springer, Berlin, pp 275–284. doi:10.1007/3-540-47789-6_29

28. Nakamura M, Wada S, Mikami T, Kitabatake A, Karino T (2002) A computational fluid mechanical study on the effects of opening and closing of the mitral orifice on a transmitral flow velocity profile and an early diastolic intraventricular flow. JSME Int J Ser C 45(4):913–922

29. Ebbers T, Bolger AF, Wranne B, Karlsson M, Wigström L (2002) Noninvasive measurement of time-varying three-dimensional relative pressure fields within the human heart. J Biomech Eng 124(3):288–293. doi:10.1115/1.1468866

30. Saber N, Wood N, Gosman AD, Merrifield R, Yang G-Z, Charrier C, Gatehouse P, Firmin D (2003) Progress towards patient-specific computational flow modeling of the left heart via combination of magnetic resonance imaging with computational fluid dynamics. Ann Biomed Eng 31(1):42–52. doi:10.1114/1.1533073

31. Long Q, Merrifield R, Yang G, Kilner P, Firmin D, Xu X (2003) The influence of inflow boundary conditions on intra left ventricle flow predictions. J Biomech Eng 125(6):922–927

32. Usyk TP, McCulloch AD (2003) Relationship between regional shortening and asynchronous electrical activation in a three-

dimensional model of ventricular electromechanics. J Cardiovasc Electrophysiol 14:S196–S202. doi:10.1046/j.1540.8167.90311.x

33. Kerckhoffs RCP, Faris OP, Bovendeerd PHM, Prinzen FW, Smits K, McVeigh ER, Arts T (2003) Timing of depolarization and contraction in the paced canine left ventricle. J Cardiovasc Electrophysiol 14:S188–S195. doi:10.1046/j.1540.8167.90310.x

34. Kilner PJ, Yang G-Z, Wilkes AJ, Mohiaddin RH, Firmin DN, Yacoub MH (2000) Asymmetric redirection of flow through the heart. Nature 404(6779): 759–761. http://www.nature.com/nature/journal/v404/n6779/suppinfo/404759a0_S1.html

35. Saber N, Gosman AD, Wood N, Kilner P, Charrier C, Firmin D (2001) Computational flow modeling of the left ventricle based on in vivo MRI data: initial experience. Ann Biomed Eng 29(4):275–283. doi:10.1114/1.1359452

36. Watanabe H, Sugiura S, Kafuku H, Hisada T (2004) Multiphysics simulation of left ventricular filling dynamics using fluid-structure interaction finite element method. Biophys J 87(3):2074–2085

37. Domenichini F, Pedrizzetti G, Baccani B (2005) Three-dimensional filling flow into a model left ventricle. J Fluid Mech 539:179–198. doi:10.1017/S0022112005005550

38. Pedrizzetti G, Domenichini F (2005) Nature optimizes the swirling flow in the human left ventricle. Phys Rev Lett 95(10):108101. doi:10.1103/PhysRevLett.95.108101

39. Lee J, Niederer S, Nordsletten D, Grice IL, Smail B, Kay D, Smith N (2009) Coupling contraction, excitation, ventricular and coronary blood flow across scale and physics in the heart. Philos Trans R Soc A 367(1986):2311–2331. doi:10.1098/rsta.2008.0311

40. Nordsletten DA, Niederer SA, Nash MP, Hunter PJ, Smith NP (2011) Coupling multi-physics models to cardiac mechanics. Prog Biophys Mol Biol 104(1–3):77–88

41. Lassila T, Malossi ACI, Stevanella M, Votta E, Redaelli A, Deparis S (2012) Multiscale fluid–structure interaction simulation of patient-specific left ventricle fluid dynamics with fictitious elastic structure regularization. Int J Numer Methods Biomed Eng 00:1–23. doi:10.1002/cnm

42. Temam R (2001) Navier–Stokes equations: theory and numerical analysis. AMS Chelsea Publishing, Providence

43. Fluid–Structure Interaction (2013) http://www.ansys.com/Products/Simulation+Technology/Fluid+Dynamics/Fluid+Dynamics+Products/ANSYS+Fluent/Features/Fluid%E2%80%93Structure+Interaction. Accessed 25 Oct 2013

44. Huerta A, Liu WK (1998) Viscous flow with large free surface motion. Comput Methods Appl Mech Eng 69(3):277–324

45. Donea J, Huerta A, Ponthot J-P, Rodrı́guez-Ferran A (2004) Arbitrary Lagrangian–Eulerian methods. Encyclopedia of computational mechanics, vol 1. Wiley, New York

46. Patankar SV, Spalding DB (1972) A calculation procedure for heat, mass and momentum transfer in 3-D parabolic flows. Int J Heat Mass Transf 15:1787–1806

47. Bronzino JD (1999) The biomedical engineering handbook, 2nd edn. CRC Press, Boca Raton

48. Bronzino JD (2006) Biomedical engineering fundamentals, 3rd edn. CRC Press, Boca Raton

49. Waite L, Schulz S, Szabo G, Vahl CF (2000) A lumped parameter model of left ventricular filling-pressure waveforms. Biomed Sci Instrum 36:75–80

50. Courtois M, Kovács SJ Jr, Ludbrook PA (1988) Transmitral pressure–flow velocity relation. Importance of regional pressure gradients in the left ventricle during diastole. Circulation 78(3):661–671. doi:10.1161/01.CIR.78.3.661

51. Nagueh SF, Appleton CP, Gillebert TC, Marino PN, Oh JK, Smiseth OA, Waggoner AD, Flachskampf FA, Pellikka PA, Evangelisa A (2009) Recommendations for the evaluation of left ventricular diastolic function by echocardiography. Eur J Echocardiogr 10(2):165–193. doi:10.1093/ejechocard/jep007